

Lensing of gravitational waves: universal signatures in the beating pattern

Oleg Bulashenko and Helena Ubach

*Departament de Física Quàntica i Astrofísica, Institut de Ciències del Cosmos (ICCUB),
Facultat de Física, Universitat de Barcelona, Martí i Franquès 1, E-08028 Barcelona, Spain.*

(Dated: December 22, 2021)

When gravitational waves propagate near massive objects, their paths curve resulting in gravitational lensing, which is expected to be a promising new instrument in astrophysics. If the time delay between different paths is comparable with the wave period, lensing may induce beating patterns in the waveform, and it is very close to caustics that these effects are likely to be observable. Near the caustic, however, the short-wave asymptotics associated with the geometrical optics approximation breaks down. In order to describe properly the crossover from wave optics to geometrical optics regimes, along with the Fresnel number, which is the ratio between the Schwarzschild diameter of the lens and the wavelength, one has to include another parameter - namely, the angular position of the source with respect to the caustic. By considering the point mass lens model, we show that in the two-dimensional parameter space, the nodal and antinodal lines for the transmission factor closely follow hyperbolas in a wide range of values near the caustic. This allows us to suggest a simple formula for the onset of geometrical-optics oscillations which relates the Fresnel number with the angular position of the source in units of the Einstein angle. We find that the mass of the lens can be inferred from the analysis of the interference fringes of a specific lensed waveform.

Keywords: Gravitational waves; Gravitational lensing; Diffraction

CONTENTS

I. Introduction	1
II. Wave approach to gravitational lensing	2
A. Thin-lens approximation	3
B. Fresnel-Kirchhoff diffraction	3
C. Characteristic scales and dimensionless parameters	4
D. Phase function. Fresnel number	4
E. Full-wave solution for the transmission factor	6
III. Geometrical optics approximation	6
IV. Full-wave vs geometrical optics	7
A. Nodal and antinodal lines	7
B. Transmission factor vs frequency	8
C. Transmission factor vs source location y	10
V. Lensed waveform	11
A. Ringdown source	11
B. Beating frequencies	11
C. Beating amplitudes	12
D. Extraction of the lens mass	14
VI. Summary	15
Acknowledgments	15
References	15

I. INTRODUCTION

When an electromagnetic or gravitational wave emitted by a distant cosmological source travels across the

Universe to reach our detectors, its path is perturbed by a gravitational field, i.e., by the geometry of spacetime. This is called gravitational lensing—the phenomenon first attributed to the bending of light due to gravity. Nowadays, this is regarded as an indispensable tool in astrophysics, with applications ranging from detecting exoplanets to constraining the distribution of dark matter and determining cosmological parameters [1, 2].

To date, only the lensing of electromagnetic (EM) waves has been confidently observed. However, since the first direct detection of gravitational waves (GWs) in 2015 [3], and the subsequent registration of about 90 new GW events by LIGO and Virgo [4–6], the gravitational lensing of GWs has become the focus of investigation (see [7, 8] and references therein). As the sensitivities of GW detectors improve, and upcoming new detector facilities join the network in the near future (with a wide-range frequency scale from nano-Hz to kHz [9–12]) the gravitational lensing of GWs is expected to be a promising new instrument in astrophysics.

From the point of view of wave optics, the lensing is manifested in different ways, depending on the ratio between the wavelength λ and the Schwarzschild radius R_S of the gravitational lens [13–15]. When $\lambda \gg R_S$, no lensing is expected since waves pass around the lens. In the opposite limit, $\lambda \ll R_S$, one would expect either magnification [16–18] or multiple images of GWs [19–25]. The latter means the detection of mutually time-delayed signals coming from the same source but taking different paths on opposite sides of the lens. The most interesting situation however is the intermediate case, $\lambda \lesssim R_S$, for which the interference between the images is expected to occur [15, 26–39].

In this paper, we address the problem of gravitational lensing from a general full-wave optics perspective [40] paying special attention to the conditions under which

the interference between the virtual images is essential. With the aim of finding some universal signatures in the interference pattern appropriate for the creation of templates for interferometric measurements, we consider the most generic lens model—the point mass lens (also called Schwarzschild lens). This is suitable for lens objects like stars, black holes (BHs), compact dark matter clumps, etc., whose dimensions are much smaller than the Einstein radius—the relevant lengthscale in gravitational lensing—and it is widely used for both EM [1, 2] and GW lensing [15, 29, 31–34, 37, 38].

Within the point mass lens (PML) model we analyze in detail the transition from wave optics to geometrical optics (GO) regimes in a two-dimensional space of characteristic parameters. It should be noted that the customary condition considered in the literature for the GO limit [15, 23, 27, 28], $\lambda \ll R_S$, breaks down near the caustic [25, 26, 41, 42]. Indeed, when the source approaches the line of sight (a caustic point for the PML), the time delay between the images becomes infinitesimally small, which means one needs infinite frequencies ($\lambda \rightarrow 0$) to reach the GO limit. In order to describe properly the crossover from wave optics to geometrical optics, along with the ratio $2R_S/\lambda$, it is necessary to include in the analysis another parameter—the angular position of the source with respect to the caustic. By analyzing the transmission factor in a two-dimensional space of parameters, we find a simple analytical relation for the onset of geometrical-optics oscillations under strong lensing conditions. On the other hand, the interference is frequency dependent in a way that depends on the lens mass. We show that in a certain range of parameters, it is possible to infer the mass of the lens from the analysis of interference fringes in the frequency domain of the lensed waveform.

The presented analysis for the transmission factor is not restricted to gravitational lensing of GWs, it can also be applied to the lensing of EM waves or any scalar waves in the PML geometry. Recently, it was pointed out that “diffractive gravitational lensing” can be used to probe as yet undiscovered astrophysical objects like primordial BHs or ultra-compact dark matter minihalos, made up for instance of QCD axions. In this investigation, different frequency ranges of EM are explored: from femtolensing of gamma ray bursts (GRBs) [43–45], and optical microlensing [46, 47] to radiowaves of fast radio bursts (FRBs) [48, 49]. It should be noted, however, that for GWs, due to their longer wavelengths and the coherence preserved over cosmological distances, the wave optics effects are more substantial than those for EM waves. In the latter case, the interference can also be washed out by the incoherent nature of EM waves emitted from different parts of an extended source [28, 43].

This paper is organized as follows. In Sec. II, we review the Fresnel-Kirchhoff approach for the diffraction of scalar waves on a thin gravitational lens and introduce the characteristic parameters for the time and frequency scales. To characterize the relevance of wave optics ef-

fects, we define a two-dimensional phase function at the lens plane (phase screen) and introduce the Fresnel number ν as a crucial parameter for the analysis of contribution of partial waves to the transmission factor. The geometrical optics limit is discussed in Sec. III. In Sec. IV we provide a detailed analysis of the transmission factor and demonstrate that the lines of local maxima and minima in the interference pattern can be regarded as constant-phase lines between two GO rays and they can be approximated by hyperbolas in a wide range of values near the caustic. The nodal and antinodal lines, when the source position is fixed, lead to the oscillation pattern uniformly spaced over the frequency, and similarly, when the frequency of the wave is fixed, the oscillations are uniformly spaced over the source position. The topological (Morse) phase shift between the images can be extracted from the width of the central maximum. We also show that the full-wave and the GO approximation start practically to coincide when the “optical path difference” between the GO rays is equal to λ . This allows us to suggest a simple formula for the onset of geometrical-optics oscillations which relates the Fresnel number with the angular position of the source in units of the Einstein angle. Finally, in Sec. V we study the effect of gravitational lensing on the ringdown waveform. The interference between the images is manifested as beating fringes in the frequency domain of the lensed waveform. From the analysis of the fringes one can infer the mass of the lens. The conclusions are summarized in Sec. VI.

II. WAVE APPROACH TO GRAVITATIONAL LENSING

In this section, we review some aspects of wave effects in gravitational lensing, which are relevant for our analysis. Let us consider the gravitational waves propagating under the gravitational potential of the lens object. The metric of the Minkowskian spacetime disturbed by the lens is given by [1]

$$ds^2 = - \left(1 + \frac{2U}{c^2}\right) c^2 dt^2 + \left(1 - \frac{2U}{c^2}\right) dr^2, \quad (1)$$

where $U(\mathbf{r})$ is the gravitational potential of the lens ($|U|/c^2 \ll 1$). The propagation of electromagnetic as well as gravitational waves (in an appropriately chosen gauge) can be described to the leading order by a scalar wave equation when the effect of lensing on polarization is negligible [50, 51]. Decomposing the scalar field into Fourier modes

$$\varphi(\mathbf{r}, t) = \int_{-\infty}^{\infty} \tilde{\varphi}(\mathbf{r}, \omega) e^{-i\omega t} \frac{d\omega}{2\pi}, \quad (2)$$

one obtains the wave equation for the scalar amplitude $\tilde{\varphi}(\mathbf{r}, \omega)$ in the frequency domain [13]

$$\left(\nabla^2 + \frac{\omega^2}{c^2}\right) \tilde{\varphi} = \frac{4\omega^2}{c^4} U \tilde{\varphi}, \quad (3)$$

which is known in wave-optics physics as an inhomogeneous Helmholtz equation.

A. Thin-lens approximation

The gravitational lens geometry is depicted in Fig. 1, where d_L , d_S , and d_{LS} are the distances of the lens and the source from the observer, and of the source from the lens, respectively. In a thin-lens approximation, the lensing occurs in a relatively small region as compared to the cosmological distances travelled by the waves, d_L , d_{LS} , d_S . Under this approximation, the lens mass is projected onto the lens plane L . Hence, the waves are assumed to propagate freely outside the lens and interact with a two-dimensional gravitational potential at the lens plane where the trajectory is suddenly deflected [1]. Figure 1 shows the path of one of the partial waves (blue line) emitted by the source S , which is deflected at the point Q of the lens and then arrives to the observer at P . The apparent angle of arrival θ differs from the real angular location of the source θ_S due to the effect of lensing. Then, in the full-wave optics approach, we must take into account all the partial waves emitted by the source, which impact the lens plane at different places, but arrive at the same point P where the total wave field is detected.

B. Fresnel-Kirchhoff diffraction

The basic idea of the Huygens-Fresnel theory is that the wave field at the observation point P arises from the superposition of secondary waves that proceed from the lens surface (see Fig. 1). Provided that the radius of curvature of the wavefront at the lens plane is large compared to the wavelength, and the angles involved are small, the wave field at the observer P can be written in the form of the Fresnel-Kirchhoff diffraction integral over the surface of the lens [40]

$$\tilde{\varphi}(P) = \frac{A}{i\lambda} \iint \frac{1}{rs} e^{i[k(r+s)+\psi_L]} dS, \quad (4)$$

where A is the scalar amplitude of the emitted wave, $\lambda = 2\pi/k$ is the wavelength, r and s are the distances indicated in Fig. 1, and ψ_L is the gravitational phase shift due to the lensing potential which will be defined later on. It is seen, that the lens acts on the wave as a transparent phase screen: passing through the lens, each partial wave acquires the phase shift ψ_L which depends on the impact parameter and therefore varies over the surface. The wavefront after the lens is disturbed due to this phase shift ψ_L , hence the diffraction effects appear at the observation point. As Fresnel pointed out in his classical work [52, 53], in order to produce the phenomena of diffraction “all that is required is that a part of the wave should be retarded with respect to its neighbouring

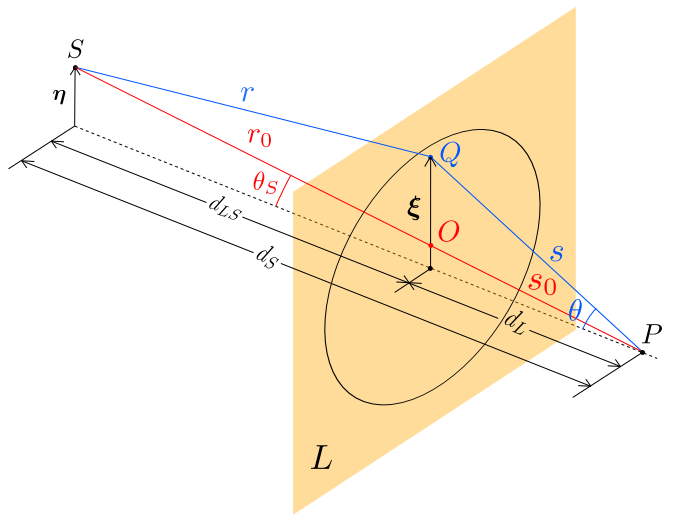


FIG. 1. Schematic diagram of gravitational lensing in a thin-lens approximation. The lens plane L is orthogonal to the optical axis (shown by dashes). A partial wave (shown in blue) emitted by the source S is scattered at the point Q of the lens before it arrives to the observer at P . In the absence of the lens, this wave would follow the unperturbed path SOP shown in red. Other notations are explained in the text.

parts.” This is precisely what happens in the lensing effect.

As the element dS explores the domain of integration in the integral (4), the factor $1/(rs)$ is the slowly changing function (due to $r, s \gg \lambda$), and it can be replaced by $1/(r_0 s_0) \approx 1/(d_L d_{LS})$ and taken away of the integral. The rapidly oscillating exponent, in contrast, should be calculated more carefully. It is convenient to add and subtract the unlensed path $r_0 + s_0$ in the phase to obtain

$$\tilde{\varphi}(P) = \frac{A}{i\lambda} \frac{e^{ik(r_0+s_0)}}{d_L d_{LS}} \iint e^{i[k\Delta l + \psi_L]} dS \quad (5)$$

where $\Delta l = r + s - r_0 - s_0$ is the geometrical path difference between the lensed and unlensed partial waves. The unlensed wave field at the point P can be written as

$$\tilde{\varphi}_0(P) = \frac{A}{d_S} e^{ik(r_0+s_0)} \quad (6)$$

where, due to $d_S \gg \lambda$, we replaced $1/(r_0 + s_0)$ by $1/d_S$ in the pre-exponential factor.

It is convenient to define the transmission factor (which is called the transmission function in Ref. [40] and the amplification factor in Ref. [27]) as the ratio between the lensed and unlensed GW amplitudes at the point P

$$F = \frac{\tilde{\varphi}(P)}{\tilde{\varphi}_0(P)} = \frac{1}{i\lambda} \frac{d_S}{d_L d_{LS}} \iint e^{i[k\Delta l + \psi_L]} dS. \quad (7)$$

Following Ref. [1], the geometrical path difference Δl can be expressed to the leading order (Fresnel expansion)

through the source position vector $\boldsymbol{\eta}$ in the source plane (see Fig. 1) and the location of a running vector $\boldsymbol{\xi}$ on the lens plane

$$\Delta l(\boldsymbol{\xi}, \boldsymbol{\eta}) = \frac{d_S}{2d_L d_{LS}} \left(\boldsymbol{\xi} - \frac{d_L}{d_S} \boldsymbol{\eta} \right)^2, \quad (8)$$

whereas the gravitational phase shift is given by

$$\psi_L(\boldsymbol{\xi}) = -\frac{4Gk}{c^2} \int \Sigma(\boldsymbol{\xi}') \ln |\boldsymbol{\xi} - \boldsymbol{\xi}'| d^2 \boldsymbol{\xi}' \quad (9)$$

where Σ is the surface mass density of the lens. For the point mass, which is a prototype of compact lens objects, it is given by $\Sigma = M \delta^2(\boldsymbol{\xi}')$.

If no gravitational lens is present on the pathway from the source to the observer, i.e. $\psi_L = 0$, the geometrical path difference Δl is the only function which affects the phases of partial waves. For this case, it can be verified, that the integral (7) gives obviously $|F| = 1$, which is in accordance with the Huygens-Fresnel principle and the definition of the transmission factor.

C. Characteristic scales and dimensionless parameters

Lensing effects are expected to be significant only when the lens is located very close to the line of sight, i.e., the source, lens, and observer are all aligned within approximately the Einstein angle, $\theta_E = R_E/d_L$, where

$$R_E = \sqrt{2R_S \frac{d_L d_{LS}}{d_S}} \quad (10)$$

is the Einstein radius and $R_S = 2GM/c^2$ is the Schwarzschild radius of the lens of mass M . Accordingly, it is convenient to normalize the angles θ and θ_S (see Fig. 1) by the Einstein angle θ_E and introduce dimensionless vectors \mathbf{x} and \mathbf{y} which determine the location of the running vector and the position of the source, respectively, at the lens plane, as follows [1]:

$$\mathbf{x} = \frac{\boldsymbol{\theta}}{\theta_E} = \frac{\boldsymbol{\xi}}{R_E}, \quad \mathbf{y} = \frac{\boldsymbol{\theta}_S}{\theta_E} = \frac{d_L}{d_S} \frac{\boldsymbol{\eta}}{R_E}. \quad (11)$$

After rescaling (11), the phase function in the exponent of the integral (7) takes on the form

$$k\Delta l + \psi_L = \omega \frac{2R_S}{c} \left[\frac{1}{2}(\mathbf{x} - \mathbf{y})^2 - \psi(\mathbf{x}) + \psi_0 \right], \quad (12)$$

where $\psi = -\psi_L/(2R_S k)$ is the scaled phase shift due to the lensing potential. For the PML it is simply $\psi(\mathbf{x}) = \ln|\mathbf{x}|$. The phase is defined up to an arbitrary constant ψ_0 which does not alter the absolute value of the transmission factor $|F|$ we are interested in.

It is seen from Eq. (12) that the time scale is determined by

$$t_M = \frac{2R_S}{c}, \quad (13)$$

which is the crossing time of the Schwarzschild diameter. Thus, to the leading order, the time delay depends only on the mass of the lens and is practically independent of the distances either to the source or to the lens:

$$t_M \simeq 2 \times 10^{-5} \text{ s} \left(\frac{M}{M_\odot} \right). \quad (14)$$

Introducing the dimensionless frequency

$$\nu = \left(\frac{\omega}{2\pi} \right) t_M, \quad (15)$$

the transmission factor (7) can finally be written as

$$F = -i\nu \iint e^{2\pi i \nu \tau(\mathbf{x}, \mathbf{y})} d^2 \mathbf{x} \quad (16)$$

in which the dimensionless scalar function

$$\tau(\mathbf{x}, \mathbf{y}) = \frac{1}{2}(\mathbf{x} - \mathbf{y})^2 - \psi(\mathbf{x}) + \psi_0 \quad (17)$$

can be associated with the Fermat potential [1] (also called time-delay function [27]). It represents retardation of partial waves to arrive at the observation point due to either the geometrical time delay (the first term) or gravitational one (the second term). Again, for $\psi(\mathbf{x}) = 0$ (no lensing), the transmission factor (16) is just $|F| = 1$.

It should be noted that the cosmological expansion can also be included in the derivation. This leads to the replacement of the lens mass M with $M_{z_L} \equiv M(1 + z_L)$, where z_L is the redshift of the lens. The distances d_L , d_S , and d_{LS} should then be interpreted as angular-diameter distances [1], for which in general $d_S \neq d_L + d_{LS}$.

D. Phase function. Fresnel number

The parameter ν introduced in Eq. (15) is a measure of the importance of diffraction effects in gravitational lensing¹. This can be seen by analyzing the partial contributions to the transmission factor from different parts of the lens. As the element $d^2 \mathbf{x}$ in the integral (16) explores the domain of integration, the phase in the exponent oscillates with a rate determined by ν . To visualize this effect, we define a phase function $\Phi(\mathbf{x})$ on a two-dimensional domain at the lens plane

$$\Phi(\mathbf{x}) = \arg \left[e^{2\pi i \nu \tau(\mathbf{x}, \mathbf{y})} \right], \quad -\pi \leq \Phi \leq \pi \quad (18)$$

with $\mathbf{x} = (x, x')$, and which depends parametrically on the source position \mathbf{y} . We plot this function for different values of ν by contrasting two cases: when the gravitational potential is turned off (Fig. 2) and when it is turned on (Fig. 3). If no lens is present, the lines of

¹ it is related to the parameter w used in Ref. [27] by $w = 2\pi\nu$

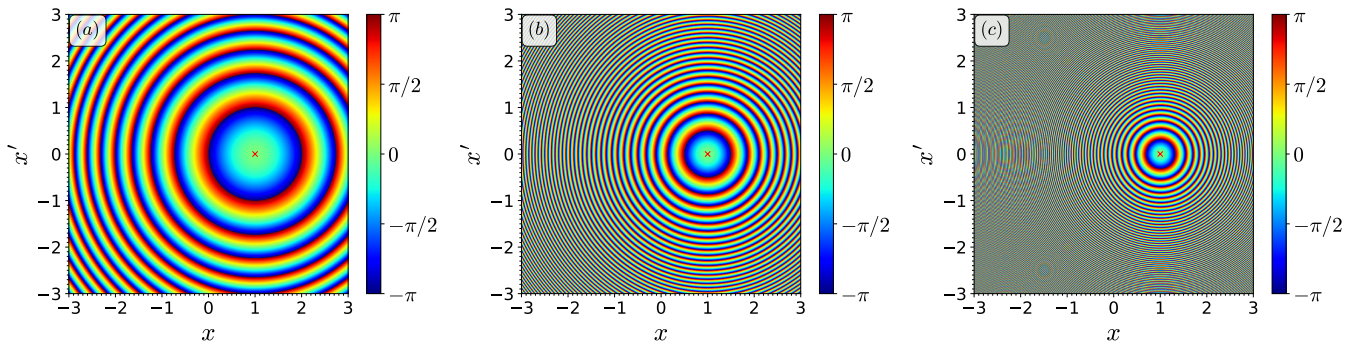


FIG. 2. Phase function (18) over the lens plane for zero gravitational potential for different values of the Fresnel number: (a) $\nu = 1$, (b) $\nu = 4$, (c) $\nu = 10$. The source located at $(1, 0)$ is shown by a red 'x'. The value of its phase is chosen to be zero. The coordinates (x, x') are in units of the Einstein radius R_E .

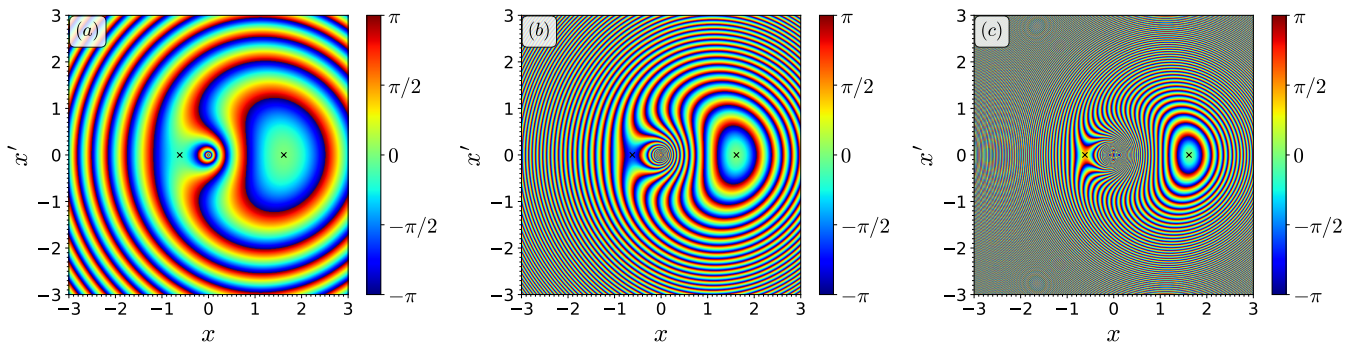


FIG. 3. Phase function (18) over the lens plane for PML gravitational potential for different values of the Fresnel number: (a) $\nu = 1$, (b) $\nu = 4$, (c) $\nu = 10$. The source located at $(1, 0)$ produces two images (shown by black 'x') at $(x_1, 0)$ and $(x_2, 0)$ with $x_{1,2} = (1 \pm \sqrt{5})/2$. They correspond to the minimum and the saddle point, respectively, of the time-delay function. The value of the phase of the first image is chosen to be zero. The coordinates (x, x') are in units of the Einstein radius R_E .

constant phase are circles concentric around the (undisturbed) source at $\mathbf{x} = \mathbf{y}$. These circles, by design, are related to Fresnel zones [40, 54]. Indeed, for a perfect alignment, $\mathbf{y} = 0$, the radii R_m of the successive Fresnel zones at the lens plane can be defined as [54]

$$m \frac{\lambda}{2} = R_m^2 \frac{d_S}{2d_L d_{LS}}, \quad m = 1, 2, 3, \dots \quad (19)$$

Hence, the areas of the zones, i.e., of the rings between successive circles, are all equal to the area of the first zone, $\pi(R_{m+1}^2 - R_m^2) = \pi R_1^2 \equiv \pi R_F^2$, where we define

$$R_F = \sqrt{\lambda \frac{d_L d_{LS}}{d_S}}, \quad (20)$$

which is the radius of the first Fresnel zone. Consequently, the number of Fresnel zones covered by the circle of the Einstein radius is just the parameter ν introduced in Eq. (15)

$$\nu = \frac{R_E^2}{R_F^2} = \frac{2R_S}{\lambda}, \quad (21)$$

which we call the Fresnel number. The higher ν , the more phase oscillations occur inside the Einstein ring of

radius R_E (the unit of length in Fig. 2).

For the case of lensing, when the gravitational potential is taken into account, the rotational symmetry is broken and multiple images appear at the lens plane (for the PML case, two images are seen in Fig. 3). It is clear that for $\nu \sim 1$, i.e., $\lambda \sim 2R_S$, all the partial waves coming from the lens contribute to the transmission factor. If however, the Fresnel number is large, $\nu \gg 1$, $|F|$ is mainly determined by small vicinities of the stationary points of the time delay function (virtual images of the source), whereas the contributions from other parts of the lens are cancelled out by destructive interference. In this limit, the GO approximation should be accurate (if y is not too close to the caustic, as will be discussed below).

It is also interesting to note that the Fresnel number (21) for the PML is independent of the distance from the lens to the observer, while in case of lensing on a topological defect like a cosmic string, it does depend on the distance [55–58].

E. Full-wave solution for the transmission factor

Equation (16) can be solved analytically for some simple geometries. In the particular case of PML, the transmission factor is obtained as [1, 13]

$$F = e^{\frac{1}{2}\pi s} e^{is \ln(s)} \Gamma(1 - is) {}_1F_1(is; 1; isy^2), \quad (22)$$

where we denoted for brevity $s \equiv \pi\nu$, $\Gamma(z)$ is the Gamma function, and ${}_1F_1(a, b, z)$ is the confluent hypergeometric function. It is interesting to note that the wave equation for the point mass lens coincides with the time-independent Schrödinger equation for Coulomb scattering [13, 14]. This means that the GWs will follow the same paths that charged particles would follow (at the lowest order) in a scattering experiment with an attracting Coulomb force. The exact solution for the latter was found by W. Gordon [59] (see also [60]) and it coincides with solution for scalar waves obtained from the Fresnel-Kirchhoff integral [1]. For the absolute value of the transmission factor one gets [13]

$$|F| = \left(\frac{2\pi^2\nu}{1 - e^{-2\pi^2\nu}} \right)^{1/2} |{}_1F_1(i\pi\nu; 1; i\pi\nu y^2)|, \quad (23)$$

which is finally a function of just two dimensionless quantities: the frequency (Fresnel number) ν and the source location y . In Fig. 4 we depict the density plot of $|F|$ in the two-dimensional parameter space (ν, y) . The figure

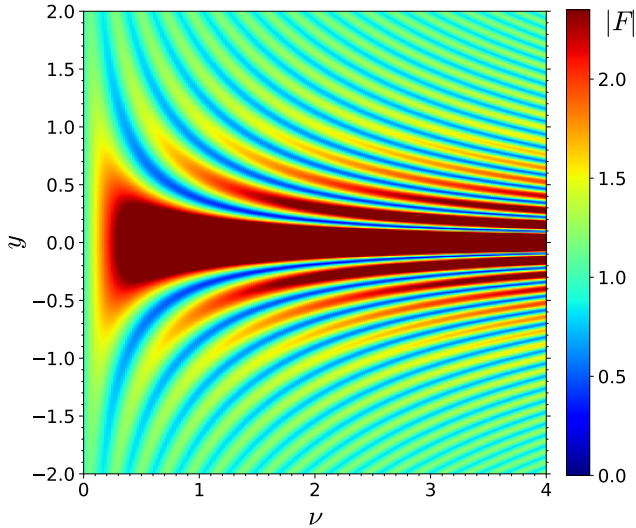


FIG. 4. Full-wave transmission factor $|F|$ given by Eq. (23) for the PML model, as a function of the Fresnel number ν and source location y .

shows clear signatures of the two-beam interference pattern. For example, the local maxima and minima form continuous lines which look like hyperbolas and correspond, as will be confirmed in the subsequent section, to lines of constant phase between two GO rays coming from virtual images.

III. GEOMETRICAL OPTICS APPROXIMATION

To understand how the interference pattern in Fig. 4 is formed, we consider the stationary phase approximation of the Fresnel-Kirchhoff integral (16) for which the main contribution comes from the stationary points of the Fermat potential (17), which are the solutions of

$$\nabla_x \tau(\mathbf{x}, \mathbf{y}) = 0. \quad (24)$$

These solutions correspond precisely to the geometrical optics rays coming from the images of the source (the GO limit). The transmission factor can then be written as a sum over these stationary points [1, 26, 27]:

$$F_{GO} = \sum_j |\mu_j|^{1/2} e^{i(2\pi\nu \tau(\mathbf{x}_j, \mathbf{y}) - n_j \pi/2)}, \quad (25)$$

where $\mu_j = (\det(\partial\mathbf{y}/\partial\mathbf{x}_j))^{-1}$ is the magnification of the j -th image and $n_j = 0, 1, 2$ is the Morse index for a minimum, saddle point and maximum of τ , respectively. The positions of the images \mathbf{x}_j are determined by the lens equation (24)

$$\nabla_x \left[\frac{1}{2}(\mathbf{x} - \mathbf{y})^2 - \psi(\mathbf{x}) \right] = \mathbf{x} - \mathbf{y} - \nabla_x \psi(\mathbf{x}) = 0 \quad (26)$$

which is just the Fermat's principle. For the PML model this equation gives $\mathbf{y} = \mathbf{x} - \mathbf{x}/|\mathbf{x}|^2$. Without loss of generality we assume that $\mathbf{y} = (y, 0)$ with $y > 0$ (the axes can always be rotated). Thus the lens equation will have two solutions: $\mathbf{x}_{1,2} = (x_{1,2}, 0)$, which correspond to two images with positions on the lens plane

$$x_{1,2} = \frac{1}{2}(y \pm \sqrt{y^2 + 4}) \quad (27)$$

and magnification

$$\mu_{1,2} = \frac{1}{4} \left(\frac{y}{\sqrt{y^2 + 4}} + \frac{\sqrt{y^2 + 4}}{y} \pm 2 \right). \quad (28)$$

Taking into account that $x_1 > 0$ and $x_2 < 0$, one can define the parameter

$$v \equiv \frac{x_1 - |x_2|}{x_1 + |x_2|} = \frac{y}{\sqrt{y^2 + 4}}, \quad (29)$$

where $0 < v < 1$ when $0 < y < \infty$. In terms of this parameter the magnification for each image can be written as

$$\mu_{1,2} = \frac{1}{4} \left(v + \frac{1}{v} \pm 2 \right) = \frac{1}{4} \left(\sqrt{v} \pm \frac{1}{\sqrt{v}} \right)^2 \quad (30)$$

and it is seen that μ_1 and μ_2 are both positive. For the PML model which has two images (minimum and saddle point), the transmission factor (25) becomes

$$F_{GO} = \sqrt{\mu_1} e^{i\varphi_1} + \sqrt{\mu_2} e^{i\varphi_2 - i\varphi_M}, \quad (31)$$

where $\varphi_i = 2\pi\nu\tau(x_i, y)$ is the phase of each image and $\varphi_M = \pi/2$ is the Morse (topological) phase shift of the second image (saddle point). Thus, we get

$$F_{GO} = (\sqrt{\mu_1} + \sqrt{\mu_2} e^{2i\alpha}) e^{i\varphi_1}, \quad (32)$$

with

$$\alpha = \pi\nu\tau_{21} - \pi/4, \quad (33)$$

which depends on the time delay between the two images $\tau_{21} \equiv \tau(x_2, y) - \tau(x_1, y)$. For the latter we obtain

$$\tau_{21} = \frac{2v}{1-v^2} + \ln\left(\frac{1+v}{1-v}\right) \equiv \tau_{geom} + \tau_{grav}. \quad (34)$$

It takes into account two effects: the geometrical time delay (the first term) and the gravitational one, or Shapiro delay (the second term). It is clear that $\tau_{21} > 0$ since x_1 corresponds to the minimum travel time. The absolute value (squared) of the transmission factor (32) can finally be written as

$$\begin{aligned} |F_{GO}|^2 &= \mu_1 + \mu_2 + 2\sqrt{\mu_1\mu_2} \cos 2\alpha \\ &= v \sin^2 \alpha + (1/v) \cos^2 \alpha \\ &= \frac{y^2 + 4 \cos^2 \alpha}{y\sqrt{y^2 + 4}}. \end{aligned} \quad (35)$$

It should give an interference pattern for which the fringe spacing is determined by α , while the minimum and maximum values of $|F_{GO}|^2$ are equal to v and $1/v$, respectively. Another important observation is that the beating oscillations can be significantly amplified and their amplitude is more pronounced for small values of y when the source approaches the caustic. Strictly at $y = 0$, Eq. (35) is not valid since it diverges. The smallest value of y for which the GO approximation is still accurate will be obtained from the full-wave solution in the next section and it depends on ν .

For small y we can expand (34) in Taylor series to obtain:

$$\tau_{21}(y) = 2y + \frac{1}{12}y^3 + O(y^5). \quad (36)$$

In Fig. 5 we compare the time delay (34) with its asymptotic approximation (36) and we also present the geometrical and gravitational partial contributions for completeness. It is clearly seen that for $0 < y \lesssim 0.5$ (strong lensing) one can safely take only the leading-order term, $\tau_{21} \approx 2y$, whereas for $0.5 \lesssim y \lesssim 1.5$ the next-order term is needed, $\tau_{21} \approx 2y + y^3/12$, to reproduce the exact value with sufficiently high accuracy. These approximations substantially simplify the analytical treatment of the transmission factor in subsequent chapters. The rather wide range of validity of $\tau_{21} \approx 2y$ can be explained by the fact that the cubic terms coming from the geometrical and gravitational delays mutually almost compensate each other being of the opposite sign. The factor of 2 is a consequence of equal contributions from geometrical and gravitational parts to the linear term.

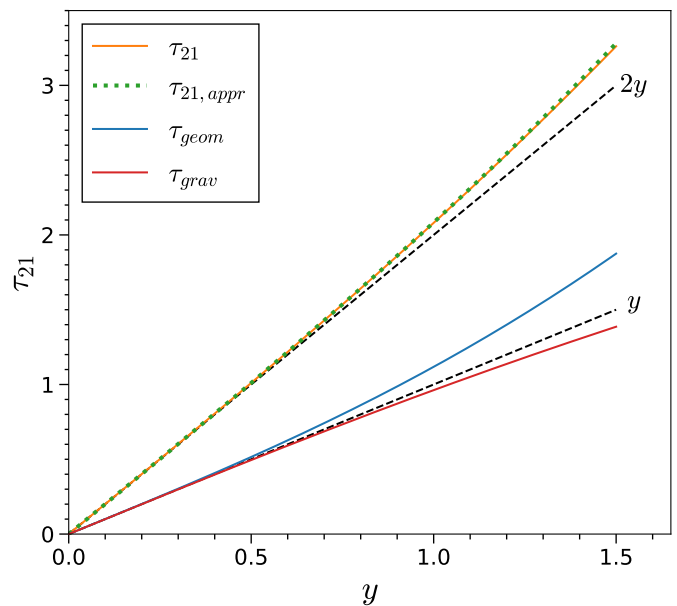


FIG. 5. Time delay τ_{21} given by Eq. (34) as a function of the source location y (orange line). It is composed of geometrical (blue line) and gravitational (red line) constituents. The asymptotic approximations are shown for comparison: at first order $\tau_{21} \approx 2y$, and at the next order $\tau_{21} \approx 2y + y^3/12$ (green dotted line).

IV. FULL-WAVE VS GEOMETRICAL OPTICS

Next we compare in Fig. 6 the GO transmission factor (35) with the full-wave solution (23). It is seen that the interference fringes are well reproduced by GO rays in the whole parameter space except at small values of ν . We also expect the discrepancy between the figures (not seen in the density plots) in the region close to the caustic $y = 0$ where the GO approximation diverges.

A. Nodal and antinodal lines

The lines of local maxima and minima in the interference pattern can be easily understood if we regard them as constant-phase lines (nodal and antinodal lines [57, 58]) which appear due to interference between two GO rays. Indeed, to have constructive or destructive interference, the maxima and minima occur when the “optical path difference” $c\Delta t_{21}$ between the GO rays can be written in terms of wavelength λ as follows

$$c\Delta t_{21} = \begin{cases} n\lambda + \frac{\lambda}{4}, & \text{at maxima,} \\ n\lambda + \frac{\lambda}{2} + \frac{\lambda}{4}, & \text{at minima} \end{cases} \quad (37)$$

with $n = 0, 1, 2, \dots$. Here, the additional term $\lambda/4$ takes into account the Morse phase shift $\pi/2$ between two stationary points—the minimum and the saddle point—as follows from Eq. (25) (see also Fig. 3). Taking into account that $c\Delta t_{21} = 2R_S\tau_{21} = \lambda\nu\tau_{21}$ and substituting

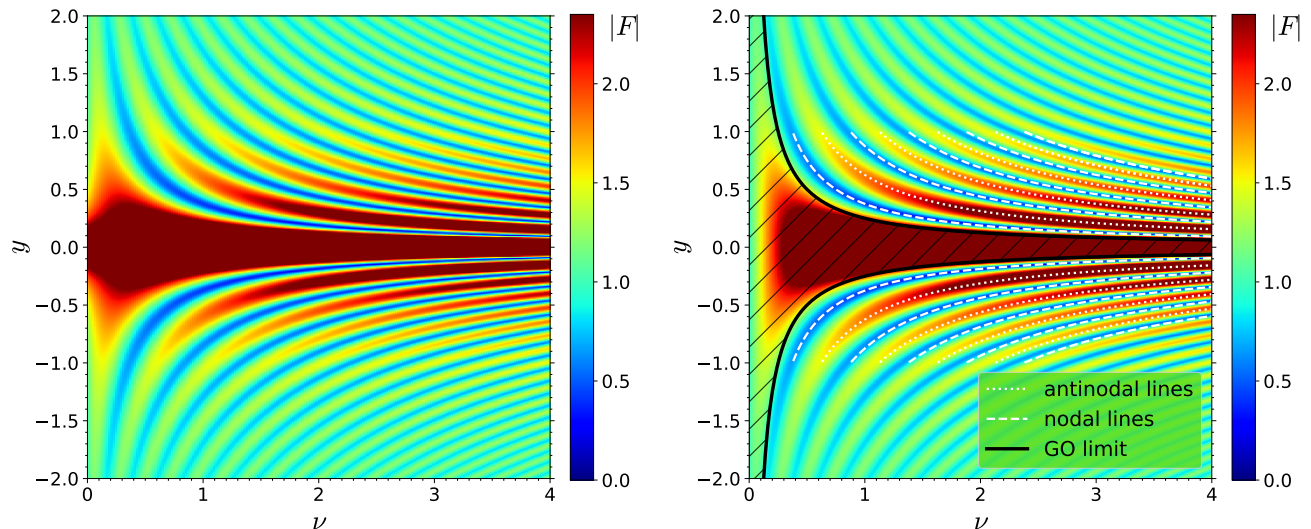


FIG. 6. Wave pattern for the transmission factor $|F|$ calculated for the PML as a function of frequency ν and source location y : (a) geometrical-optics (GO) approximation; (b) full-wave solution with superimposed lines of constant phase between GO rays (white dotted and dashed lines). The excluded masked region where the GO approximation is not valid is bounded by a black line.

$\tau_{21} \approx 2y$, we obtain

$$y_n = \frac{1}{2\nu} \cdot \begin{cases} (n + \frac{1}{4}), & \text{at maxima,} \\ (n + \frac{3}{4}), & \text{at minima,} \end{cases} \quad (38)$$

which are hyperbolas in (ν, y) parameter space. Alternatively, the same formulas can formally be obtained by assuming that the phase α in Eq. (35) satisfies

$$\alpha = \begin{cases} \pi n, & \text{at maxima,} \\ \frac{\pi}{2} + \pi n, & \text{at minima.} \end{cases} \quad (39)$$

The hyperbolas (38) are shown in Fig. 6(b) superimposed on the wave pattern (shown in color) obtained from full-wave solution (23) (the same as in Fig. 4). A good agreement is observed for a rather wide range of the source location² that validates the approximation $\tau_{21} \approx 2y$ for strong lensing at $0 < y \lesssim 0.5$.

B. Transmission factor vs frequency

To get more insight into how the transition from full-wave to GO approximation occurs, we present in Fig. 7 plots of $|F(\nu)|$ for some fixed values of the source position y (horizontal sections of Fig. 6). This would correspond to a situation when the relative displacement of the lens and the source is negligible during the observational time, which for ground-based GW detectors is

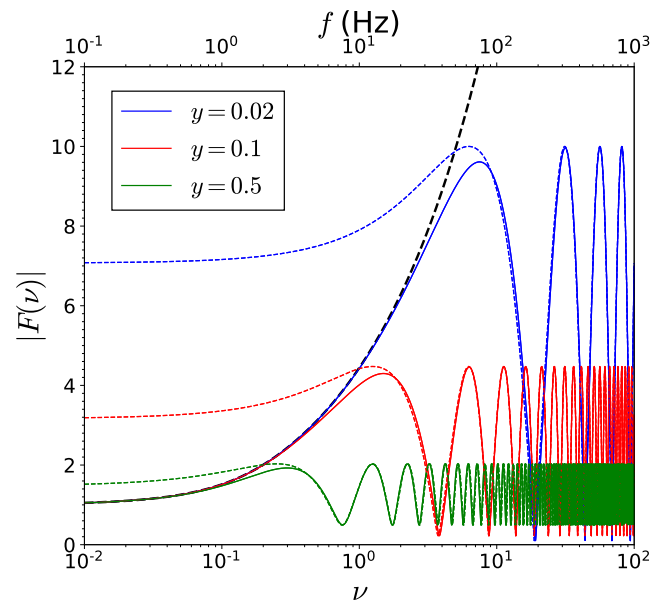


FIG. 7. Transmission factor $|F(\nu)|$ vs frequency for different angular locations of the source: $y = \theta_S/\theta_E = 0.02; 0.1; 0.5$. Solid lines correspond to the full-wave solution (23) and dashed lines, represented by the same colour, to the GO approximation (35). The asymptotic low-frequency curve (40) is shown by black dashes. The bottom horizontal axis shows the dimensionless frequency (or Fresnel number) ν defined in Eqs. (15) and (21), and the top axis maps into a physical GW frequency f (in Hz) in the LIGO/Virgo band for a specific choice of lens mass $M = 5 \times 10^3 M_\odot$.

² we only omit the very first line of maximum for $n = 0$ which is outside the region of the GO validity.

\lesssim seconds, while for space-based detectors and pulsar timing arrays can reach larger timescales, \lesssim years. It is

seen from Fig. 7 that at low frequencies (small Fresnel numbers ν), the GO approximation substantially overestimates the transmission factor, that means the regions of the lens other than the GO images (stationary points) contribute significantly and the stationary phase approximation does not hold. As a result the amplification is suppressed. In this limit, full-wave solutions should be used which are seen to converge to a unique asymptotic curve

$$|F(\nu)|_{\max} = \left(\frac{2\pi^2\nu}{1 - e^{-2\pi^2\nu}} \right)^{1/2}, \quad (40)$$

which is obtained from (23) in the limit $\nu y \rightarrow 0$. Note that Eq. (40) represents also the transmission factor for the particular case $y = 0$, when the source, lens and observer are perfectly aligned. It gives the maximum amplification that the GWs may achieve for each frequency.

In the opposite limit of high frequencies, the full-wave solutions asymptotically coalesce into the corresponding GO curves and one can observe quite similar oscillation patterns for different y . To describe in more detail the transition from wave optics to GO regime, we define some characteristic frequencies in Fig. 8 where $|F(\nu)|$ is depicted for a particular value of $y = 0.1$. We distinguish the following regions of interest:

(i) Diffraction region, $\nu \lesssim \nu_D$.

In this region the wavelength λ is too large with respect to the Schwarzschild radius, so the lens does not affect the propagation of waves, $|F| \approx 1$ for any y . To estimate the upper limit of this region, we expand the function (40) at small arguments $|F(\nu)|_{\max} = 1 + \frac{1}{2}\pi^2\nu + O(\nu^2)$, to obtain $\nu_D \ll 2/\pi^2$, so $\nu_D \simeq 0.01$ is a reasonable value.

(ii) Amplification region, $\nu_D \lesssim \nu < \nu_1^+$.

This region extends from ν_D up to the first maximum and it is characterized by a monotonic magnification without oscillations as ν increases. Although the full-wave and GO solutions still have a discrepancy at the first maximum, the values of ν are close, so for simplicity we can take as the upper limit of this region the first GO maximum given by Eq. (38) for $n = 0$ at $\nu_1^+ = 1/(8y)$. As ν increases, the full-wave solution follows closely the asymptotic curve (40) in the interval: $\nu_D \lesssim \nu \lesssim \nu_A$, where the point of separation ν_A can be estimated by applying to Eq. (23) the asymptotic expansion ${}_1F_1(i\pi\nu; 1; i\pi\nu y^2) \approx J_0(2\pi\nu y) = 1 - \pi^2\nu^2 y^2 + O(\nu^4 y^4)$, where the Bessel function J_0 is expanded at small arguments. The full-wave solution starts to deviate from $|F(\nu)|_{\max}$ when the second term in the expansion is non-negligible. This happens approximately at $\pi^2\nu_A^2 y^2 \simeq 0.03$, so $\nu_A \simeq \sqrt{0.03}/(\pi y) \simeq 0.055/y$. It is seen that the value of ν_A increases as y decreases, in accordance with Fig. 7.

(iii) GO oscillation region, $\nu > \nu_G$.

We define ν_G as a threshold frequency at which the full-wave and GO solutions start practically to coincide. As seen from the figure, it should be in between

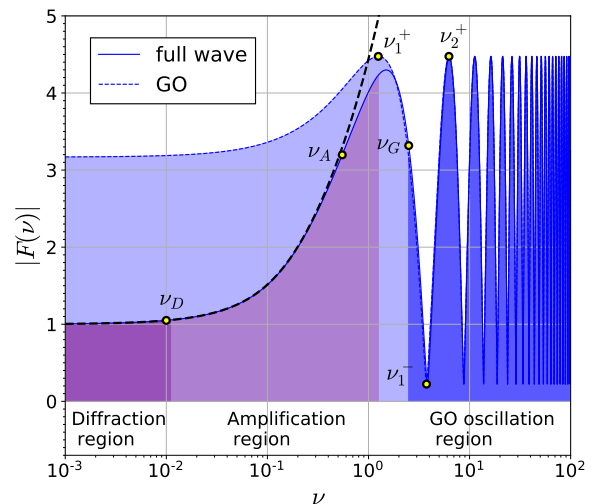


FIG. 8. Transmission factor $|F(\nu)|$ vs dimensionless frequency (Fresnel number) ν for the source location at $y = 0.1$. The full-wave and the GO solutions are compared. The asymptotic low-frequency curve (40) is shown by black dashes. Characteristic frequencies and regions are indicated.

the first maximum $\nu_1^+ = 1/(8y)$ and the first minimum $\nu_1^- = 3/(8y)$, so we define it for simplicity in the middle,

$$\nu_G = \frac{1}{4y}, \quad (41)$$

that corresponds to the condition: $c\Delta t_{21}|_{\nu=\nu_G} = \lambda/2$. It is important to note that the onset of the GO validity is inversely proportional to the source location y : the smaller value of y , the higher the corresponding frequency ν_G . In the limit $y \rightarrow 0$, one gets $\nu_G \rightarrow \infty$, this means that for the line of sight the GO approximation is never valid, since $y = 0$ corresponds to the caustic point. The region of the GO validity in the two-parameter space (ν, y) is indicated in Fig. 6(b).

We can further simplify our analytical treatment by taking into account that the range $\nu > \nu_G$ with $y \lesssim 0.5$ is of the most interest, since for these values two images are well pronounced, they are of comparable intensity and the interference pattern is strongly amplified. In this case, by expanding the GO solution (35) we obtain a reduced analytical formula

$$|F_{GO}|^2 \approx \frac{y}{2} + \left(\frac{2}{y} - \frac{y}{4} \right) \cos^2 \left[2\pi\nu y - \frac{\pi}{4} \right], \quad (42)$$

which reproduces quite well the oscillation pattern. Note that for any fixed $y \neq 0$, the function $|F(\nu)|$ oscillates with evenly spaced maxima and minima. The values of minima are equal to $y/2$ (to the leading order). They are not zero because the interference is not completely destructive when the source is off the line of sight and the images are therefore of different magnifications. The amplitude of the oscillations (the difference between maximum and minimum values) increases $\sim 2/y$ when $y \rightarrow 0$

(see Fig. 7). These oscillations appear due to crossing the nodal and antinodal lines—the constant-phase lines between the GO rays—when ν varies (Fig. 6). As will be shown below, they also determine the interference fringe in the GW lensed waveform. The fringe spacing over the spectrum is uniform with the characteristic interval

$$\Delta\nu = \frac{1}{\tau_{21}(y)} \approx \frac{1}{2y}, \quad (43)$$

i.e., to the leading order, it is inversely proportional to the parameter y . Translating into physical units, the frequency spacing of the fringe is determined by

$$\Delta f = \frac{1}{2t_M} \left(\frac{\theta_E}{\theta_S} \right) \simeq 2.5 \times 10^4 \text{ Hz} \left(\frac{M_\odot}{M} \right) \left(\frac{\theta_E}{\theta_S} \right). \quad (44)$$

For $y = 0.5$ and $M = 100M_\odot$ this gives $\Delta f = 500$ Hz.

C. Transmission factor vs source location y

Another situation of interest is the case of a continuous monochromatic signal coming for instance from (i) an isolated neutron star emitting GWs at frequencies within the LIGO/Virgo band, or (ii) a supermassive black hole (SMBH) binary in their long inspiral phase, so that their frequencies can be considered to be almost constant for a long time [61]. The GWs emitted by the latter sources fall in the frequency band of the space interferometer LISA and pulsar timing arrays (PTA) experiments. In this situation, we assume that ν is approximately constant, but the angular parameter y changes with time due to the relative displacement of the source, lens, or observer [23, 32, 47, 49].

Fig. 9 shows a comparison of the transmission factor $|F|$ as a function of y calculated in the full-wave optics regime and the GO limit, for fixed values of ν . It is seen that the interference pattern is perfectly reproduced by the GO limit for $|y| > y_G$, where $y_G = 1/(4\nu)$ is defined similar to ν_G in Sec. IV B. The fringe spacing is uniform over the source location y with the characteristic interval

$$\Delta y \approx \frac{1}{2\nu} = \frac{\lambda}{4R_S}, \quad (45)$$

i.e., it is proportional to the wavelength λ and inversely proportional to the mass of the lens. It is interesting to note, that the central maximum contains an additional information on the topological phase shift between the two images, since it is wider (see Fig. 9). By calculating its width from Eq. (38) as twice the distance between zero and the nearest minimum, we obtain

$$\Delta y_c = \frac{3}{4\nu} = \Delta y + \frac{1}{4\nu} = \frac{3\lambda}{8R_S} \quad (46)$$

where the fringe spacing Δy is given by Eq. (45). It is seen that the central maximum is wider than the rest of

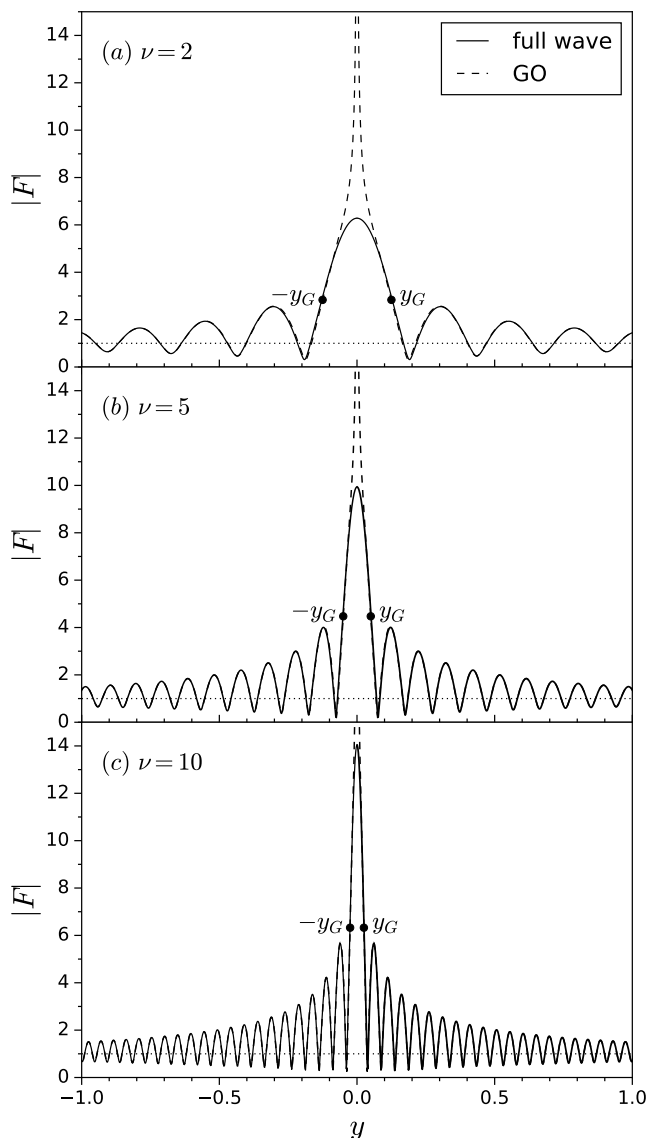


FIG. 9. Transmission factor $|F|$ vs source location $y = \theta_S/\theta_E$ for different Fresnel numbers $\nu = 2; 5; 10$. The full-wave solutions (23) are compared with the GO approximations (35).

the fringe spacing. The additional $1/4\nu$ comes precisely from the Morse phase shift $\pi/2$ of the saddle point image.

At $y \rightarrow 0$, where the GO approximation fails, one can simplify the full-wave solution (23) by applying the Bessel function approximation [13], ${}_1F_1(i\pi\nu; 1; i\pi\nu y^2) \approx J_0(2\pi\nu y)$. One gets

$$|F(\nu, y)| \approx (2\pi^2\nu)^{1/2} J_0(2\pi\nu y). \quad (47)$$

It is also assumed that $e^{-2\pi^2\nu}$ in (23) is negligible for relevant frequencies $\nu \gtrsim 0.3$. As Fig. 10 shows, Eq. (47) nicely approximates the full-wave solution at low values of y where the GO approximation does not hold.

Summarizing this section, the validity of the GO limit

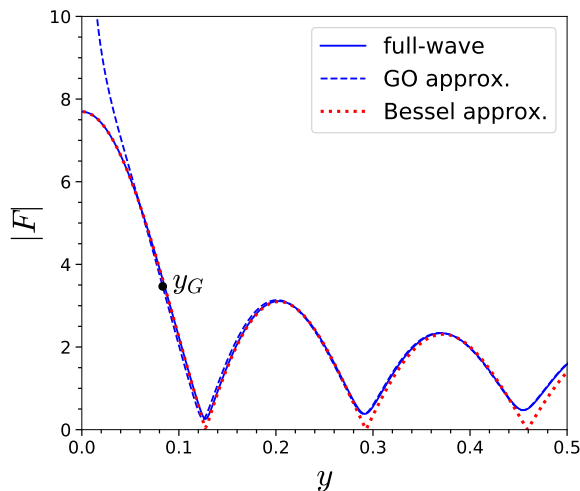


FIG. 10. Transmission factor $|F|$ vs source location y for $\nu = 3$. The full-wave solution (23) is compared with the Bessel approximation (47), valid at small y , and the GO approximation (35), valid for $y > y_G$.

can be defined as

$$\nu y \gtrsim \frac{1}{4}, \quad (48)$$

i.e., for a fixed mass of the lens and source position, the wavelength λ should satisfy the condition

$$\lambda \lesssim \lambda_G, \quad \lambda_G = 8R_S \left(\frac{\theta_S}{\theta_E} \right). \quad (49)$$

Thus, the condition for the onset of the GO oscillations depends not only on the ratio between the wavelength λ and the Schwarzschild radius R_S , but also on the angular location of the source θ_S (in units of the Einstein angle θ_E).

V. LENSED WAVEFORM

In previous sections we have analyzed the transmission factor for a monochromatic signal. Let us now study how a waveform with a given frequency distribution originating from a distant GW source is modified by gravitational lensing. Since we are interested in wave optics effects, our aim is to investigate how the interference between images is imprinted in the lensed waveform.

Given that we deal with a linear equation for wave propagation, the gravitationally lensed waveform $\tilde{h}_L(\omega)$ registered by the interferometer in the frequency domain should be the product [15, 27]

$$\tilde{h}_L(\omega) = \tilde{h}(\omega) F(\omega), \quad (50)$$

where $\tilde{h}(\omega)$ is the waveform emitted by the source (unlensed) and $F(\omega)$ the transmission factor of the lens.

A. Ringdown source

To simplify analytical treatment, we consider a simple waveform with carrier frequency ω_0 modulated by exponentially decaying function. This waveform may be associated with the dominant quasi-normal mode of the last stage of a binary BH merger, called ringdown [62, 63]. The unlensed amplitude for $t > 0$ is given by

$$h(t) = h_0 e^{-\Gamma t} \cos(\omega_0 t), \quad (51)$$

where Γ is the inverse of the damping time and h_0 is the initial magnitude. For the ringdown model the parameters $\omega_0 = 2\pi f_0$ and Γ are mutually related [63]

$$f_0 \simeq 1.207 \times 10^4 \text{ Hz} \left(\frac{M_\odot}{M_S} \right), \quad \Gamma \simeq 1.496 \cdot f_0 \quad (52)$$

and depend on the mass of the source M_S . Nevertheless, one could study a more general case as well, when those parameters are independent. The Fourier transform of the unlensed waveform (51) is

$$\tilde{h}(\omega) = \int_{-\infty}^{\infty} h(t) e^{i\omega t} dt = \frac{\tilde{h}_0 (\Gamma - i\omega)}{(\Gamma - i\omega)^2 + \omega_0^2}, \quad (53)$$

which has a peak close to the carrier frequency $\omega = \omega_0$. The value $\tilde{h}_{\max} \equiv \tilde{h}(\omega_0)$ is convenient to use for normalization of the waveform, so that $\tilde{h}_L(\omega)/\tilde{h}_{\max}$ will be a measure of amplification in the frequency domain due to lensing. As a unit of frequency, it is suitable to introduce the ringdown frequency of the source ω_0 . Thus, $\tilde{\omega} \equiv \omega/\omega_0$ will be the dimensionless Fourier frequency.

For calculations, we use the full-wave transmission factor given by Eq. (23) for which the variable ν is translated to the dimensionless frequency $\tilde{\omega}$ by $\nu = \nu_0 \tilde{\omega}$, where

$$\nu_0 = f_0 t_M = \frac{2R_S}{\lambda_0} \quad (54)$$

is the Fresnel number corresponding to the wavelength $\lambda_0 = 2\pi c/\omega_0$ of the source. By its definition, ν_0 is the key wave-optics parameter, which controls the appearance of interference effects. Since the source frequency ω_0 is determined by the source mass M_S , the parameter ν_0 can also be expressed as the ratio of the masses of the lens and the source [substituting the values from (14) and (52)]:

$$\nu_0 \simeq 0.24 \frac{M}{M_S}. \quad (55)$$

We can expect the interference fringe in the lensed waveform whenever the time delay between the images t_M is comparable with the GW period $T_0 = 1/f_0$. Later on, we will specify more precise conditions.

B. Beating frequencies

As a first example, consider $\nu_0 = 5/4$, that corresponds to the lens mass $M \simeq 5M_S$. For this case, the effect of

gravitational lensing on the ringdown waveform is illustrated in Fig. 11. The interference between two images is manifested as beating fringes in the frequency domain. The frequencies corresponding to the maxima and minima of the signal can be obtained analytically from the constant-phase lines (38)

$$\tilde{\omega}_n = \frac{1}{2\nu_0 y} \cdot \begin{cases} (n + \frac{1}{4}), & \text{maxima,} \\ (n + \frac{3}{4}), & \text{minima,} \end{cases} \quad (56)$$

with $n = 0, 1, 2, \dots$. It is easy to see that the values in Fig. 11 are in agreement³ with the analytical formulas (56). Indeed, for $y = 0.1$ the minima are at $\tilde{\omega}_n = 4n + 3 = 3; 7; 11; 15; \dots$, while for $y = 0.05$ they are at $\tilde{\omega}_n = 2(4n + 3) = 6; 14; 22; \dots$. In both cases the fringe frequencies are integer multiples of the ringdown frequency ω_0 because of matching (taking into account the Morse shift) between t_M and T_0 in this case. Translating into physical units, those frequencies are determined by

$$f_n = \Delta f \cdot \begin{cases} (n + \frac{1}{4}), & \text{maxima,} \\ (n + \frac{3}{4}), & \text{minima,} \end{cases} \quad (57)$$

where Δf is given by Eq. (44).

C. Beating amplitudes

The maximum and minimum values of the oscillations of the strain can also be obtained analytically by using Eq. (35) for the GO limit or its reduced formula (42). For the line joining the maxima (see dotted lines in Fig. 11) we obtain

$$\tilde{h}_{\max}(\omega) = \sqrt{H^+} \tilde{h}(\omega), \quad H^+ = \frac{\sqrt{y^2 + 4}}{y} \approx \frac{2}{y} + \frac{y}{4}, \quad (58)$$

while for the minima

$$\tilde{h}_{\min}(\omega) = \sqrt{H^-} \tilde{h}(\omega), \quad H^- = \frac{y}{\sqrt{y^2 + 4}} \approx \frac{y}{2}, \quad (59)$$

where the approximations for H^\pm are valid under strong lensing $y \lesssim 0.5$ and for the frequencies satisfying the GO limit $\tilde{\omega} > 1/(4\nu_0 y)$ (equivalent to $\nu > \nu_G$ in Sec. IV B). The level of amplification of the fringe oscillations, determined as the ratio between the maximum and minimum values, is independent of the frequency

$$\mathcal{A} \equiv \frac{\tilde{h}_{\max}}{\tilde{h}_{\min}} = \sqrt{\frac{H^+}{H^-}} = \sqrt{1 + \frac{4}{y^2}} \approx \frac{2}{y}. \quad (60)$$

It increases inversely proportional to y near the caustic.

³ except $n = 0$ for the first maximum which is outside the region of the GO validity.

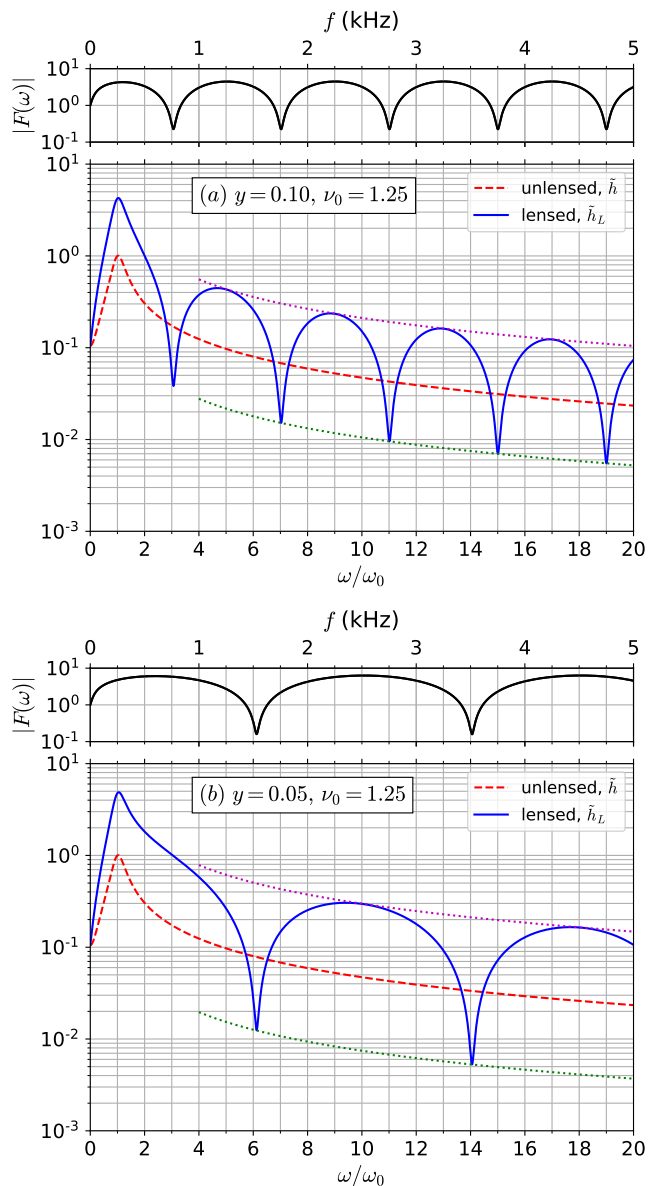


FIG. 11. Signatures of interference between two images for Fresnel number $\nu_0 = 5/4$ and two different source locations: (a) $y = 0.1$ and (b) $y = 0.05$. The upper panels of each subfigure show the transmission factor and the lower panels show the strain amplitude in the frequency domain: lensed $\tilde{h}_L(\tilde{\omega})$ vs unlensed $\tilde{h}(\tilde{\omega})$ waveform [Eq. (53)], both normalized to the unlensed peak value. The bottom horizontal axis shows the frequency in units of the source frequency ω_0 , while the top axis maps into a physical GW frequency in the LIGO/Virgo band for a specific choice of lens mass $M = 250M_\odot$. The upper envelope line (purple dots) joins the maxima [Eq. (58)] and the lower envelope line (green dots) joins the minima [Eq. (59)].

Under the strong lensing condition, $0 < y \lesssim 0.5$, one would expect significant amplification, according to Fig. 7, for $\nu \gtrsim 0.2$. As a second example, we consider the lensing for the Fresnel number $\nu_0 = 1/4$. This

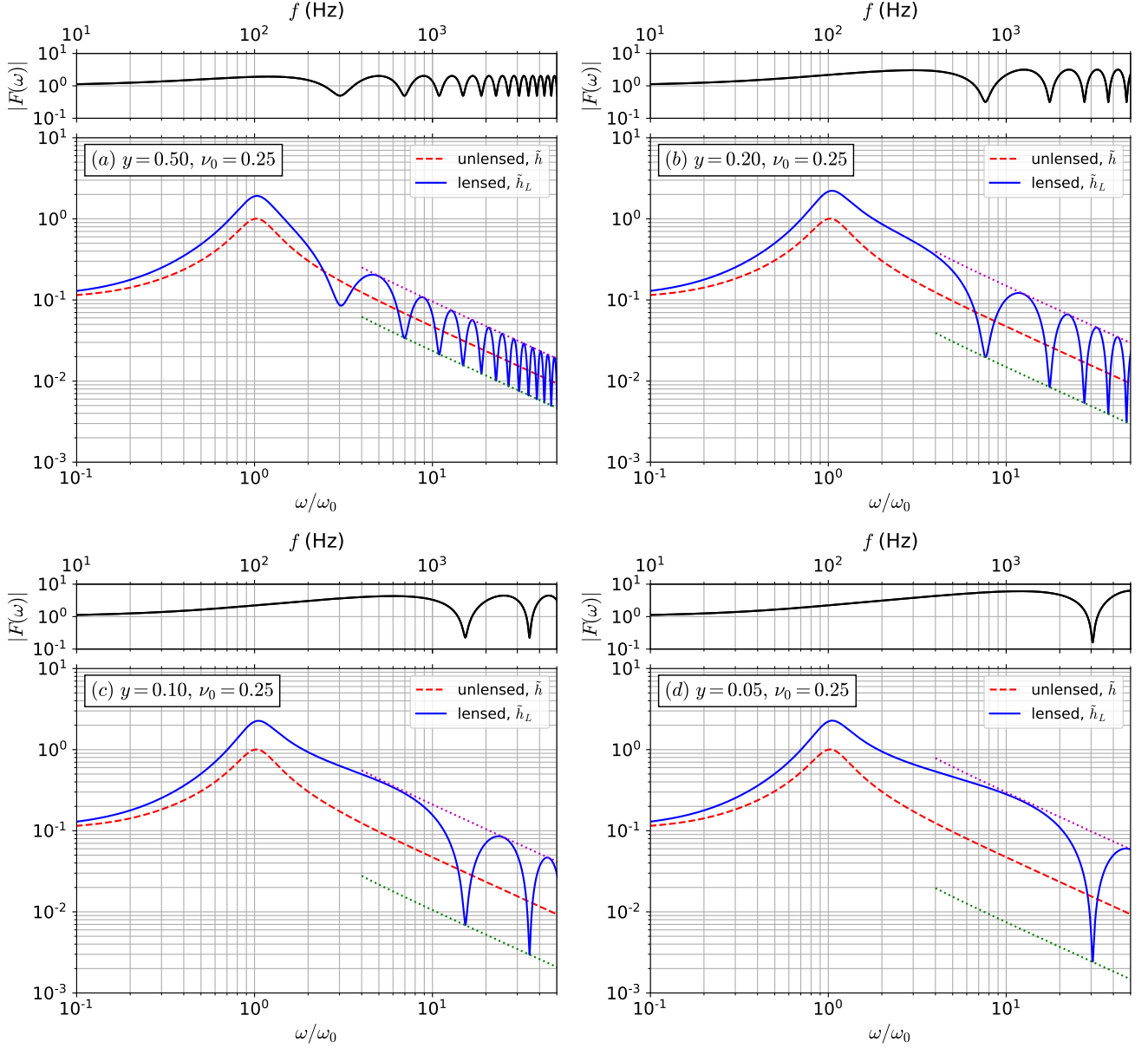


FIG. 12. Similar to Fig. 11 in log-log scale for Fresnel number $\nu_0 = 1/4$ and source locations: (a) $y = 0.5$; (b) $y = 0.2$, (c) $y = 0.1$, and (d) $y = 0.05$. In all the cases, $\nu_0 < \nu_1^+$, so the ringdown principal peak lies at the amplification region of $|F|$ and the GO oscillations appear at higher frequencies. The top axis maps into a physical frequency for the lens mass $M = 125M_\odot$.

value corresponds to the condition that the mass of the lens is approximately equal to the mass of the source, $M \simeq M_S$. The results are depicted in Fig. 12 in the log-log scale for different values of y progressively decreasing from 0.5 to 0.05 in the strong lensing regime approaching the caustic. The fringe spacing is approximately $\Delta\tilde{\omega} = 1/(2\nu_0 y) = 2/y$, i.e. inversely proportional to y . This result can be easily verified from the figure. The principal ringdown peak is amplified about the factor of 2 and its value is almost independent of y , since it is located in the “amplification region” according to Fig. 7, which occurs when $\nu_0 < \nu_1^+$. At higher frequen-

cies, the signal gets into the “GO oscillation region” for which the amplification becomes sensitive to y . From Eq. (60) we obtain the amplification ratio $\mathcal{A} \approx 4, 10, 20, 40$ for $y = 0.5, 0.2, 0.1, 0.05$, respectively in the figure. The closer the source to the caustic, the higher the amplification of the fringe oscillations. On the other hand, the smaller y , the larger the fringe spacing.

It can also happen that the principal ringdown peak falls into the GO oscillation region, when $\nu_0 > \nu_G$. This would eventually occur if the product of the two parameters fulfills the condition $\nu_0 y \geq 1/4$. For such a case, however, the identification of the unlensed peak position

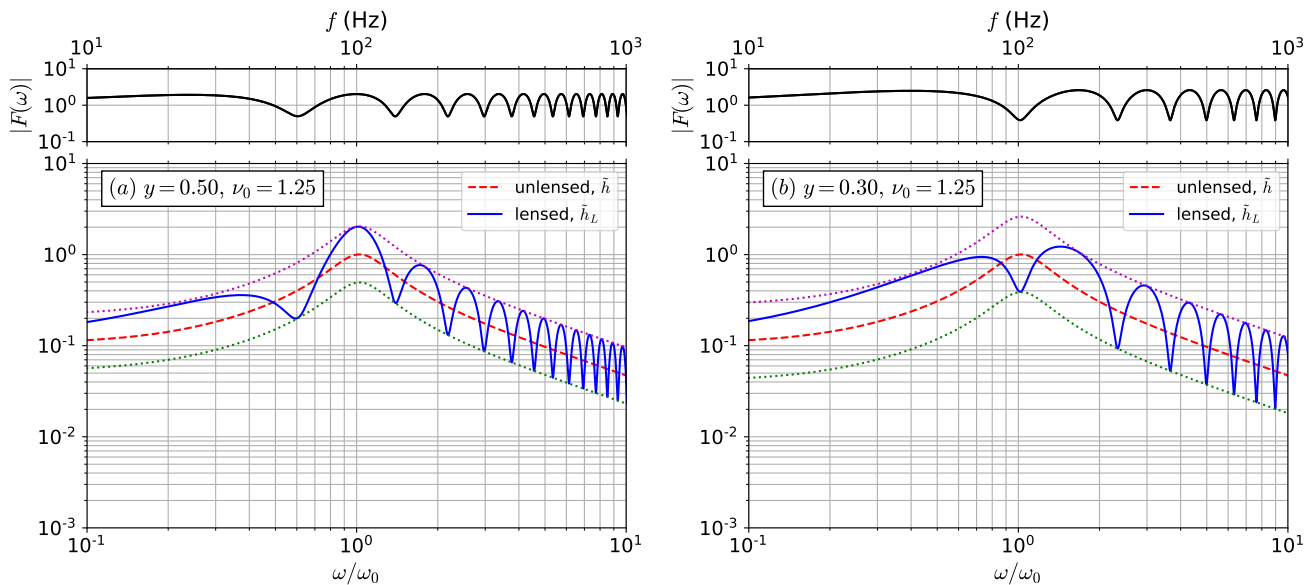


FIG. 13. Similar to Fig. 12 for Fresnel number $\nu_0 = 5/4$ and source locations: (a) $y = 0.5$; (b) $y = 0.3$, where in both cases $\nu_0 > \nu_G$, so the GO oscillations overlap with the ringdown principal peak. The upper envelope line (purple dots) joins the maxima [Eq. (58)] and the lower envelope line (green dots) joins the minima [Eq. (59)].

will be more involved, since any of the two interference conditions—constructive or destructive—may happen at the peak frequency, as shown in Fig. 13(a),(b).

D. Extraction of the lens mass

Suppose we can get independently the fringe spacing Δf and the amplification ratio $\mathcal{A} = \tilde{h}_{\max}/\tilde{h}_{\min}$ from the lensed waveform of the observational data. Then, by using Eqs. (57) and (60), we can infer the time t_M and consequently the mass of the lens directly from the measured values:

$$t_M \approx \frac{\mathcal{A}}{4\Delta f}, \quad (61)$$

$$\frac{M}{M_\odot} \approx 1.25 \times 10^4 \left(\frac{\text{Hz}}{\Delta f} \right) \mathcal{A}. \quad (62)$$

This result suggests the estimation for the lower bound of the lens mass which can be inferred via lensing effect. As an input parameter we take the high frequency cutoff f_{\max} of the detector bandwidth. In order to be able to extract information on the lens mass, one needs to observe at least one beating oscillation below the cutoff (roughly the first and the second minimum). Under this condition, from Eq. (57) we get

$$\left(\frac{M}{M_\odot} \right)_{\min} \simeq 5 \times 10^4 \left(\frac{\text{Hz}}{f_{\max}} \right) \left(\frac{1}{y} \right). \quad (63)$$

For the ground-based interferometers (LIGO, Virgo, Kagra), if we take the cutoff frequency $f_{\max} \simeq 5 \times 10^3$ Hz [9], this gives $(M/M_\odot)_{\min} \simeq 10/y$. Thus, for $y = 0.5$, the

mass $\gtrsim 20M_\odot$ and for $y = 0.1$, the mass $\gtrsim 100M_\odot$ can in principle be extracted from the lensed waveform oscillations. As for the mass of the source, since the beating conditions depend only on the lens, it is only necessary that the peak frequency of the source falls into the interferometer bandwidth.

Similar estimations can be done for space-based interferometers (LISA, DECIGO) taking $f_{\max} \simeq 1$ Hz [64]. We obtain $(M/M_\odot)_{\min} \simeq 5 \times 10^4/y$. Thus, the lower bound for the mass to be detected would be $M \gtrsim 10^5 M_\odot$ for $y = 0.5$, and $M \gtrsim 5 \times 10^5 M_\odot$ for $y = 0.1$. The intermediate-mass black holes (IMBHs) and supermassive black holes (SMBHs) [61] are possible candidates in this range for detection as a source, as well as a lens via beating pattern in the waveform.

Table I shows the fringe oscillation frequencies f_1^- , f_2^- and the amplification ratio \mathcal{A} calculated for some selected values of the lens masses M and the source masses M_S . The beating oscillations depend finally on two parameters—the mass of the lens M and the source position angle y . Stellar-mass BHs as well as IMBHs are considered as possible candidates for detection in the LIGO/Virgo bands and SMBHs for the LISA band. As previously mentioned, M should be replaced by $M_{zL} = M(1+z_L)$ for the lens at the redshift z_L . Similarly, the mass of the source M_S at the redshift z_S should be replaced by $M_S(1+z_S)$.

One can also extract the mass of the source M_S whenever the ringdown principal peak is well separated from the GO oscillations, i.e., when $\nu_0 < \nu_1^+$. In this case the lensed principal peak, even when amplified, will still be at the same frequency $\omega \approx \omega_0$ as the unlensed one (see Figs. 11 and 12). The source mass M_S can then be de-

M_S/M_\odot	$f_S(\text{Hz})$	M/M_\odot	ν_0	y	\mathcal{A}	$f_1^-(\text{Hz})$	$f_2^-(\text{Hz})$
40	300	40	1/4	0.5	4	950	2200
				0.3	6.67	1600	3700
		120	3/4	0.3	6.67	530	1200
				0.1	20	1600	3700
		200	5/4	0.1	20	950	2200
				0.05	40	1900	4400
120	100	120	1/4	0.3	6.67	530	1200
				0.1	20	1600	3700
		360	3/4	0.2	10	260	620
				0.05	40	1100	2500
		600	5/4	0.2	10	160	370
				0.05	40	640	1500
10^6	0.012	10^6	1/4	0.2	10	0.095	0.22
				0.05	40	0.38	0.89
		3×10^6	3/4	0.2	10	0.032	0.074
				0.05	40	0.13	0.3
		5×10^6	5/4	0.05	40	0.076	0.18
				0.02	100	0.19	0.44

TABLE I. The first two minima of fringe oscillations f_1^- and f_2^- [Eq. (57)] and the amplification ratio \mathcal{A} [Eq. (60)] calculated for different lens masses M and source positions y . The first set of parameters corresponds to the source of stellar mass BH with $M_S = 40M_\odot$ and different lenses, and the second set corresponds to the IMBH with $M_S = 120M_\odot$. Both sets give frequencies matching the LIGO/Virgo bands. The third set of parameters with $M_S = 10^6M_\odot$ corresponds to space-based interferometers.

duced from Eq. (52), given the model of one dominant quasi-normal mode is appropriate. When $\nu_0 > \nu_G$, the GO oscillations overlap with the peak (like in Fig. 13), so one should locate the position of the peak from the envelope of maxima (or minima).

VI. SUMMARY

We have studied the transition from full-wave optics to geometrical optics regimes for gravitational lensing on a compact-mass object (Schwarzschild lens). By analyzing the transmission factor in a two-dimensional space of characteristic parameters—the Fresnel number ν and the source location y —we distinguish three physically different regions: diffraction, amplification and geometrical-optics oscillations. From the point of view of observations, two of them—the amplification and GO-oscillations—are of interest. The latter, in addition, reveals the beating pattern in the waveform for GWs (for EM waves, in most of the cases, the oscillations are washed out due to incoherence and the small size of the wavelength with respect to the size of the source).

Our analysis suggests that the onset of the GO oscillations caused by interference between two images corresponds (with a sufficiently high accuracy) to the condition $\nu y > 1/4$, which in terms of the time delay between the images can be written as $\Delta t_{21} > T/2$, with T being the period of the GW. The above condition includes the region close to the caustic ($y \rightarrow 0$) and it is less restrictive than $\Delta t_{21} \gg T$, which is usually considered for the GO limit. Similarly to light whose intensity is greatest near caustics, one would expect the highest magnification of GWs—where the lensing effects are likely to be observable—to be close to the caustic as well. On the other hand, for $y \lesssim 0.5$ the beating pattern in the frequency domain shows universal signatures, which allow us to infer the (redshifted) mass of the lens from the amplification ratio and the spacing of the fringes [Eq. (62)]. While the lens mass can be extracted from the GO oscillations alone, the source location can only be obtained in terms of y , i.e., in units of the Einstein angle; there still remains a degeneracy in the distances [Eq. (10)]. Gravitational lensing is a good opportunity to detect the objects which do not emit, but curve the paths of the incoming waves, causing different parts of the wavefront to interfere, thereby magnifying or distorting the signal.

ACKNOWLEDGMENTS

We are grateful to Mark Gieles, Jordi Miralda Escudé, Jordi Portell i de Mora, Tomas Andrade, Ruxandra Bondarescu, and the members of the group Virgo-ICCUB for helpful discussions. H.U. acknowledges financial support from the Institute of Cosmos Sciences of the University of Barcelona (ICCUB).

-
- [1] P. Schneider, J. Ehlers, and E. Falco, *Gravitational Lenses* (Springer, New York, 1992).
[2] A.O. Petters, H. Levine, and J. Wambsganss, *Singularity Theory and Gravitational Lensing* (Birkhauser, Boston,

- 2001).
[3] B. P. Abbott et al. (LIGO Scientific and Virgo Collaborations), Observation of Gravitational Waves from a Binary Black Hole Merger, *Phys. Rev. Lett.* **116**, 061102 (2016).

- [4] B. P. Abbott et al. (LIGO Scientific and Virgo Collaborations), GWTC-1: A Gravitational-Wave Transient Catalog of Compact Binary Mergers Observed by LIGO and Virgo during the First and Second Observing Runs, arXiv:1811.12907 (2018), *Phys. Rev. X* **9**, 031040 (2019).
- [5] R. Abbott et al. (LIGO Scientific and Virgo Collaborations), GWTC-2: Compact binary coalescences observed by LIGO and Virgo during the first half of the third Observing Run. arXiv:2010.14527 (2020), *Phys. Rev. X* **11**, 021053 (2021).
- [6] R. Abbott et al. (LIGO Scientific and Virgo Collaborations), GWTC-3: Compact binary coalescences observed by LIGO and Virgo during the second part of the third Observing Run. arXiv:2111.03606 (2021).
- [7] A.K. Meena, J. S. Bagla, Gravitational lensing of gravitational waves: wave nature and prospects for detection, *Monthly Notices of the Royal Astronomical Society*, **492**, 1127 (2020).
- [8] S. Mukherjee, B.D. Wandelt, and J. Silk Probing the theory of gravity with gravitational lensing of gravitational waves and galaxy surveys, *Monthly Notices of the Royal Astronomical Society*, **494**, 1956 (2020).
- [9] *An Overview of Gravitational Waves: Theory, Sources and Detection*, edited by G. Auger and E. Plagnol (World Scientific, 2017).
- [10] M. Maggiore, C. Van Den Broeck and N. Bartolo et al., Science case for the Einstein Telescope, *Journal of Cosmology and Astroparticle Physics* **2020** 050 (2020).
- [11] E. Barausse et al. (LISA Collaboration), Prospects for fundamental physics with LISA, *Gen. Relativ. Gravit.* **52**, 81 (2020).
- [12] M. Bailes, B.K. Berger, P.R. Brady, et al., Gravitational-wave physics and astronomy in the 2020s and 2030s, *Nat. Rev. Phys.* **3**, 344 (2021).
- [13] S. Deguchi and W. D. Watson, Diffraction in gravitational lensing for compact objects of low mass, *The Astrophysical Journal*, **307**, 30 (1986).
- [14] S. Deguchi and W. D. Watson, Wave effects in gravitational lensing of electromagnetic radiation', *Phys. Rev. D* **34**, 1708 (1986).
- [15] T. T. Nakamura, Gravitational Lensing of Gravitational Waves from Inspiring Binaries by a Point Mass Lens, *Phys. Rev. Lett.* **80**, 1138 (1998).
- [16] Y. Wang, A. Stebbins, and E. L. Turner, Gravitational Lensing of Gravitational Waves from Merging Neutron Star Binaries, *Phys. Rev. Lett.* **77**, 2875 (1996).
- [17] L. Dai, T. Venumadhav, and K. Sigurdson, Effect of lensing magnification on the apparent distribution of black hole mergers, *Phys. Rev. D* **95**, 044011 (2017).
- [18] K.-H. Lai, O.A. Hannuksela, A. Herrera-Martín, J.M. Diego, T. Broadhurst, and T.G.F. Li, Discovering intermediate-mass black hole lenses through gravitational wave lensing, *Phys. Rev. D* **98**, 083005 (2018).
- [19] M. Sereno, A. Sesana, A. Bleuler, P. Jetzer, M. Volonteri, and M.C. Begelman, Strong Lensing of Gravitational Waves as Seen by LISA, *Phys. Rev. Lett.* **105**, 251101 (2010).
- [20] R. Takahashi, Arrival time differences between gravitational waves and electromagnetic signals due to gravitational lensing, *Astrophys. J.* **835**, 103 (2017).
- [21] G.P. Smith, M. Jauzac, J. Veitch, W.M. Farr, R. Massey, and J. Richard, What if LIGO's gravitational wave detections are strongly lensed by massive galaxy clusters? *Monthly Notices of the Royal Astronomical Society* **475**, 3823 (2018)
- [22] S.-S. Li, S. Mao, Y. Zhao, and Y. Lu, Gravitational lensing of gravitational waves: a statistical perspective, *Monthly Notices of the Royal Astronomical Society* **476**, 2220 (2018),
- [23] M. Oguri, Strong gravitational lensing of explosive transients, *Rep. Prog. Phys.* **82** 126901 (2019).
- [24] B. Liu, Z. Li, and Z.-H. Zhu, Complementary constraints on dark energy equation of state from strongly lensed gravitational wave, *Mon. Not. R. Astron. Soc.* **487**, 1980 (2019).
- [25] J.M. Ezquiaga, D. E. Holz, W. Hu, M. Lagos, and R.M. Wald, Phase effects from strong gravitational lensing of gravitational waves, *Phys. Rev. D* **103**, 064047 (2021).
- [26] T. T. Nakamura and S. Deguchi, Wave Optics in Gravitational Lensing, *Progress of Theoretical Physics Supplement* **133**, 137 (1999).
- [27] R. Takahashi and T. Nakamura, Wave effects in the gravitational lensing of gravitational waves from chirping binaries, *Astrophys. J.* **595**, 1039 (2003).
- [28] N. Matsunaga and K. Yamamoto, The finite source size effect and wave optics in gravitational lensing, *Journal of Cosmology and Astroparticle Physics* **2006** 023 (2006).
- [29] Z. Cao, L.-F. Li, and Y. Wang, Gravitational lensing effects on parameter estimation in gravitational wave detection with advanced detectors, *Phys. Rev. D* **90**, 062003 (2014).
- [30] L. Dai, S. S. Li, B. Zackay, S. Mao and Y. Lu, Detecting Lensing-Induced Diffraction in Astrophysical Gravitational Waves *Phys. Rev. D* **98**, 104029 (2018).
- [31] S. Jung and C. S. Shin, Gravitational-Wave Fringes at LIGO: Detecting Compact Dark Matter by Gravitational Lensing, *Phys. Rev. Lett.* **122**, 041103 (2019).
- [32] K. Liao, M. Biesiada, and X.-L. Fan, The Wave Nature of Continuous Gravitational Waves from Microlensing, *Astrophys. J.* **875**, 139 (2019).
- [33] J.M. Diego, O.A. Hannuksela, P.L. Kelly, T. Broadhurst, K. Kim, T.G.F. Li, and G.F. Smoot, Observational signatures of microlensing in gravitational waves at LIGO/Virgo frequencies, *Astronomy and Astrophysics* **627**, A130 (2019).
- [34] S. Hou, X.-L. Fan, K. Liao, and Z.-H. Zhu, Gravitational wave interference via gravitational lensing: Measurements of luminosity distance, lens mass, and cosmological parameters, *Phys. Rev. D* **101**, 064011 (2020).
- [35] D.J. D'Orazio and A. Loeb, Repeated gravitational lensing of gravitational waves in hierarchical black hole triples, *Phys. Rev. D* **101**, 083031 (2020).
- [36] S. Hou, P. Li, H. Yu, M. Biesiada, X.-L. Fan, and Z.-H. Zhu, Lensing rates of gravitational wave signals displaying beat patterns detectable by DECIGO and B-DECIGO, *Phys. Rev. D* **103**, 044005 (2021).
- [37] P. Cremonese, J. M. Ezquiaga, and V. Salzano, Breaking the mass-sheet degeneracy with gravitational wave interference in lensed events, *Phys. Rev. D* **104**, 023503 (2021).
- [38] P. Cremonese, D.F. Mota, and V. Salzano, Characteristic features of gravitational wave lensing as probe of lens mass model, arXiv:2111.01163 (2021).
- [39] H. Yu, Y. Wang, B. Seymour, and Y. Chen, Detecting gravitational lensing in hierarchical triples in galactic nuclei with space-borne gravitational-wave observatories, *Phys. Rev. D* **104**, 103011 (2021).

- [40] M. Born and E. Wolf, *Principles of Optics*, 7th ed. (Cambridge University Press, Cambridge, 1999).
- [41] M.V. Berry, Scalings for diffraction-decorated caustics in gravitational lensing, *J. Opt.* **23** 065604 (2021).
- [42] H.G. Choi, Ch. Park, S. Jung, Small-scale shear: peeling of diffuse subhalos with gravitational waves, *Phys. Rev. D* **104**, 063001 (2021).
- [43] A. Katz, J. Kopp, S. Sibiryakov, and W. Xue, Femtolensing by dark matter revisited, *Journal of Cosmology and Astroparticle Physics* **2018** 005 (2018).
- [44] S.Jung and T. Kim Gamma-ray burst lensing parallax: Closing the primordial black hole dark matter mass window, *Phys. Rev. Research* **2** 013113 (2020)
- [45] J. Paynter, R. Webster, E. Thrane, Evidence for an intermediate-mass black hole from a gravitationally lensed gamma-ray burst, *Nature Astronomy* (2021)
- [46] P. Montero-Camacho, X. Fang, G. Vasquez, M. Silva, and C.M. Hirata, Revisiting constraints on asteroid-mass primordial black holes as dark matter candidates, *Journal of Cosmology and Astroparticle Physics* **2019** 031 (2019).
- [47] S. Sugiyama, T. Kurita, and M. Takada, On the wave optics effect on primordial black hole constraints from optical microlensing search, *Monthly Notices of the Royal Astronomical Society* **493**, 3632 (2020).
- [48] A. Katz, J. Kopp, S. Sibiryakov, and W. Xue, Looking for MACHOs in the spectra of fast radio bursts, *Monthly Notices of the Royal Astronomical Society* **496**, 564 (2020).
- [49] D.L. Jow , S. Foreman, U.-L. Pen, and W. Zhu, Wave effects in the microlensing of pulsars and FRBs by point masses, *Monthly Notices of the Royal Astronomical Society* **497**, 4956 (2020).
- [50] P.C. Peters, Index of refraction for scalar, electromagnetic, and gravitational waves in weak gravitational fields, *Phys. Rev. D* **9**, 2207 (1974).
- [51] C. W. Misner and K. S. Thorne, and J. A. Wheeler, *Gravitation* (W. H. Freeman and Company, San Francisco, 1973).
- [52] A. Fresnel, Memoire sur la diffraction de la lumiere, *Mèm. Acad. Sci.* **5**, 339 (1821).
- [53] *The Wave Theory of Light: Memoirs of Huygens, Young and Fresnel*, ed. by H. Crew, (American Book Company, New York, 1900), pp. 79–144.
- [54] F.A. Jenkins and H.E. White, *Fundamentals of Optics*, 4ed, (McGraw-Hill, New York, 2001).
- [55] T. Suyama, T. Tanaka, and R. Takahashi, Exact wave propagation in a spacetime with a cosmic string, *Phys. Rev. D* **73**, 024026 (2006).
- [56] I. Fernández-Núñez and O. Bulashenko, Wave diffraction by a cosmic string, *Phys. Lett. A* **380**, 2897 (2016).
- [57] I. Fernández-Núñez and O. Bulashenko, Emergence of Fresnel diffraction zones in gravitational lensing by a cosmic string, *Phys. Lett. A* **381**, 1764 (2017).
- [58] I. Fernández-Núñez and O. Bulashenko, Wave propagation in metamaterials mimicking the topology of a cosmic string, *J. Opt.* **20** 045603 (2018).
- [59] W.Gordon, Über den Stoss zweier Punktladungen nach der Wellenmechanik, *Zeitschrift für Physik.* **48** 180 (1928).
- [60] N.F.Mott and H.S.W. Massey, *The theory of atomic collisions*, 3ed. (Oxford, Clarendon Press, 1965).
- [61] M. Maggiore, *Gravitational Waves. Vol: 2 Astrophysics and Cosmology* (Oxford University Press, Oxford, 2018).
- [62] E.E, Flanagan and S.A. Hughes, Measuring gravitational waves from binary black hole coalescences. I. Signal to noise for inspiral, merger, and ringdown, *Phys. Rev. D* **57**, 4535 (1998).
- [63] E. Berti, V. Cardoso and A.O. Starinets, Quasinormal modes of black holes and black branes, *Class. Quantum Grav.* **26** 163001 (2009).
- [64] H. Audley et al., *Laser Interferometer Space Antenna*, arXiv:1702.00786.